Yields of correlated fragment pairs in spontaneous fission of ^{252}Cf

G. M. Ter-Akopian,[1,2] J. H. Hamilton,[2] Yu. Ts. Oganessian,[1] A. V. Daniel,[1,2]
J. Kormicki,[2,*] A. V. Ramayya,[2] G. S. Popeko,[1] B. R. S. Babu,[2] Q.-H. Lu,[2]
K. Butler-Moore,[2,†] W.-C. Ma,[3] E. F. Jones,[2] J. K. Deng,[2,‡] D. Shi,[2] J. Kliman,[4] M. Morháč,[4] J. D. Cole,[5]
R. Aryaeinejad,[5] N. R. Johnson,[6] I. Y. Lee,[6,§] and F. K. McGowan[6]
[1]*Joint Institute for Nuclear Research, Dubna 141980, Russia*
[2]*Department of Physics, Vanderbilt University, Nashville, Tennessee 37235*
[3]*Department of Physics, Mississippi State University, Mississippi State, Mississippi 39762*
[4]*Institute of Physics, Slovak Academy of Sciences, Bratislava, Slovak Republic*
[5]*Idaho National Engineering Laboratory, Idaho Falls, Idaho 83415*
[6]*Physics Division, Oak Ridge National Laboratory, Oak Ridge, Tennessee 37831*
(Received 12 September 1996)

Independent yields of 139 individual secondary (appearing after neutron evaporation) fragment pairs of five different charge splits (Z_L/Z_H=46/52, 44/54, 42/56, 40/58, and 38/60) have been experimentally measured by detecting the coincidences between prompt γ rays emitted in the spontaneous fission of ^{252}Cf. Nuclear charge and mass distributions of fission fragments that follow from the measured yields of individual fragment pairs are consistent with similar previously known more integral data. Another type of data extracted from the yields of fragment pairs is the multiplicity distributions of prompt neutrons emitted in the five above charge divisions of ^{252}Cf. For the measured charge splits, about 70% of the fission events where $\geqslant$7 neutrons are evaporated from the fission fragments occur for the Mo-Ba split of ^{252}Cf. Mass and excitation energy distributions of primary Ru-Xe, Mo-Ba, and Zr-Ce fragments were deduced from a least squares fit to the yield pattern of secondary fragment pairs. For the Ru-Xe and Zr-Ce splits, the experimental data are well fitted by assuming one fission mode with average total kinetic energy $\langle$TKE$\rangle$ values close to the value of $\langle$TKE$\rangle$ known for the ^{252}Cf spontaneous fission. For the Mo-Ba split, a successful fit could be obtained only with the assumption that, in addition to this ''normal'' fission mode, a second mode with a remarkably lower value of $\langle$TKE$\rangle$ of 153 MeV contributes to this charge split. This is 36 MeV lower than for the normal mode. These data indicate that in mode two the barium nuclei are hyperdeformed (3:1 axis ratio) at scission. Mean angular momentum values of Mo-Ba fission fragments observed in pairs together with various partners have been deduced from the measured populations of different spin levels of the fragment nuclei. These angular momentum values are discussed in terms of their dependence on the primary fragment excitation energy and presence of two fission modes. [S0556-2813(97)05303-X]

PACS number(s): 25.85.Ca, 21.10.Gv, 27.60.+j, 27.90.+b

I. INTRODUCTION

We present in this paper a detailed report of our development of an approach to the study of low-energy nuclear fission and of the results obtained in studies of the spontaneous fission of ^{252}Cf as briefly reported recently [1,2]. The phenomenon of low-energy nuclear fission has a long-term history. A number of approaches to the problem have been developed, and their power has been demonstrated in a number of studies. First we present a review of previous studies, and our motivation for a new approach, and finally the more detailed results from our studies.

Since the time of the discovery of nuclear fission through the present, investigations of low-energy fission have remained a dynamic field of nuclear physics (see, [3–5]). Detailed studies of fission fragment charge, mass, and energy distributions for a large variety of fissile systems continue to be an important source of information about the mechanism of this process (see Ref. [6]). This is because the total kinetic energy (TKE) of fission fragments is mainly defined by the Coulomb (plus nuclear) potential as it appears just after scission. Therefore, TKE values, together with fragment mass asymmetry, provide information on some essential characteristics of scission configurations. Prompt fission neutrons and γ rays carry information about the excitation energy of the fission fragments and also are an important source of information about low-energy fission [7].

The asymmetric mass distributions of fission fragments have been well known for a long time, and considerable data about these distributions for different fissile nuclei have been accumulated (see Ref. [8]). It is generally recognized as seen in theoretical calculations (see Refs. [9–14]) that the mass distributions are governed by shell effects in deformed nuclei. Theory also predicted [10] the coexistence of different asymmetry modes for the fission of the same nucleus. This was observed later in experiments as the phenomenon of bimodal fission in the vicinity of lead [15] (see also Ref.

*Also at UNIRIB, ORISE, Oak Ridge, TN 37832, on leave from Institute of Nuclear Physics, Cracow, Poland.
†Current address: INEL, Idaho Falls, ID 83415.
‡Current address: Tsinghua University, Beijing, P.R. China.
§Current address: Lawrence Berkeley Lab., Berkeley, CA 94720.

 © 1997 The American Physical Society

[16]) and heavy fermium nuclei [17] (see also Ref. [18,19]). Investigations of the full course of the potential energy surface in deformation space revealed pronounced fission paths (valleys or channels) as a characteristic inherent in fission processes of many heavy nuclei [20–23]. Later, the multimodal-random-neck-rupture model was introduced by Brosa and co-workers [24]. This model allowed the authors to reproduce the mean values and variances of fragment mass (A) and total kinetic energy distributions known for different nuclei prone to low-energy fission. For spontaneous fission of ^{252}Cf [24], they extracted possible evidence for five integral channels from an analysis of a high precision two-dimensional yield distribution $Y(A,\mathrm{TKE})$ obtained for this nucleus [25]. These included three rather similar standard modes, a weak superasymmetric mode on the mass wings, and a symmetric mass superlong mode. New studies of fission channels were reported in [26–29]. The basic result of these activities was the recognition of a number of fission modes distinguished by their particular (sometimes partly overlapping) ranges of the scission point mass asymmetry and elongation.

The scission-point fission model [30], based on the assumption of equilibrium at scission, was in fact the first to reproduce, to a large extent, the basic observables of low-energy fission. Later refinements (see Refs. [28–31]) produced even more detailed results. However the answer to the fundamental question of when in the process the mass asymmetry is determined remains ambiguous.

Evidently, the solution of the problem should be sought in fission dynamics, and in this direction theory might expect from low-energy fission experiments not only more specific information about the nuclear deformation energy but also the data on couplings between different degrees of freedom at the time of the descent from saddle to scission. Widths of isobaric charge distributions were analyzed in terms of the role of zero-point oscillations of a giant dipole resonance [32] that undergoes a ''freeze out'' at a certain point depending on necking velocity [33]. Odd-even effects in the charge yields of fission fragments were used for extracting information about the amount of collective energy dissipated during the descent from saddle to scission [34]. Different authors [35–37] have shown that valuable information related to the fission dynamics follows from data on the fragment mass, energy, and nuclear charge distributions. Nevertheless, a number of important questions remain. Only an upper limit had been obtained for the fraction of the collective energy dissipated during the descent towards the scission point. It remains unclear what part of the collective energy is transformed into the quasiparticle excitations just at the neck disruption. Also, it is not clear whether the zero-point oscillations squeezed by neck formation are the only source of the isobaric charge distribution or are there other mechanisms, such as stochastic single-nucleon exchange, responsible for this distribution. There is very little experimental information about the amount of energy which goes into the excitation of collective degrees of freedom orthogonal to the fission mode [3,14]. To these questions one can add that the deviations obtained for the average nuclear charge of fission fragments from the ''unchanged-charge division'' have received only a rough explanation.[1]

In this paper we present an approach to ascertaining scission configurations, i.e., to ultimately know what are the excitation, deformation, and tip distance for fragments of a given mass and nuclear charge at scission. As is well known, these parameters define the energy partition at fission written as

$$Q(A_L,A_H)=E_{\mathrm{diss}}+E_{\mathrm{def}L}+E_{\mathrm{def}H}+\mathrm{TKE}=E_L^*+E_H^*+\mathrm{TKE}, \tag{1}$$

where $Q(A_L,A_H)$ is the full energy release at fission resulting in two primary (i.e., before neutron evaporation) fragments of mass numbers A_L and A_H(subscripts L and H stand for the light and heavy fragment, respectively, where the fragment atomic numbers are assumed to be fixed), E_{diss} is the dissipation energy, i.e., the part of the energy released at the descent from saddle to scission which is spent as heat, $E_{\mathrm{def}L(H)}$ are the deformation energies of the primary fragments at scission, and $E^*_{L(H)}$ are their excitation energy at infinity.

The previous techniques of measuring fragment mass, charge, and TKE (see Ref. [38]) have allowed one to find the masses and nuclear charges of both fragments only for the case of ''cold fragmentation'' (or ''cold compact fission'') (see [39,40]). Sometimes, identification of cold deformed fission configurations turns out well (see [41,42]). However, only qualitative conclusions could be drawn from the results gained by the observations of ''cold deformed fission.'' Furthermore, this fission mode, as well as the ''cold compact fission,'' make only a small part of the bulk of the low-energy fission events.

Access to new information, in addition to that usually obtained in previous experiments, could improve our ability to estimate the values entering into Eq. (1). One possible source of such information is spectroscopic studies of prompt characteristic γ rays emitted by fission fragments. It was shown [43] and confirmed in our earlier work [44] that the total intensities of the lowest $2^+\rightarrow 0^+$ ground-state band transitions observed in the de-excitation of even-even fission products reflect, to a high degree of accuracy ($<5\%$), the total independent yields of these isotopes. In our first brief report we showed [45] that the values of relative yields of pairs of fission fragments, as they appear after neutron evaporation, can be extracted from the analysis of γ-γ and γ-γ-γ coincidences detected for prompt fission γ rays with new larger detector arrays. This led to the first measurements of the independent yields of Zr-Ce and Mo-Ba pairs and the prompt neutron multiplicity distribution of the Mo-Ba split of ^{252}Cf ([1,2]).

Some aspects of our work have been described briefly earlier [1,44–46]. Brief reports and our more detailed analysis of the Mo-Ba charge split have been presented recently [2,47–50]. Here we report more details of our experiment and of the analysis procedures and a more complete set of data on the independent yields of different charge splits for

[1]See the definition of this term in Ref. [8] and discussions on this topic in Ref. [36].

secondary even Z fission fragment pairs (i.e., formed after neutron evaporation) obtained for the spontaneous fission of ^{252}Cf. Results were obtained for fragment pairs belonging to Pd-Te, Ru-Xe, Mo-Ba, Zr-Ce, and Sr-Nd charge splits of ^{252}Cf. Fragment pair independent yields and prompt neutron multiplicity distributions were extracted from the data. An unfolding procedure for extraction of primary fragment mass and excitation energy distributions from the obtained patterns of yields of secondary fragment pairs is described. Such distributions were extracted for the three charge splits (Ru-Xe, Mo-Ba, and Zr-Ce) for which the most extensive data exist. This analysis revealed a new second mode in the Mo/Ba split. From the new second mode which goes via very low average total kinetic energy $\langle \mathrm{TKE} \rangle$, we extract evidence that in this second mode the barium nuclei are hyperdeformed with long to short axis ratio the order of 3:1 at scission.

Other information that one can extract from our experiments include angular momenta of the fission fragments for specific fragment pairs [45]. Such data are desirable since the fragment angular momentum carry information about coupling between different collective degrees of freedom at the descent from saddle to scission [3,14,51–54]. Results and analysis of the relative intensities of γ transitions between the levels of the ground-state rotational bands of some Mo and Ba fragments appearing together with different partner fragments are discussed. Mean angular momentum values of fission fragments obtained after neutron evaporation are discussed here in terms of a model [52,53] that assumes a statistical equilibrium between collective degrees of freedom at the scission point. In summarizing our results, we also propose prospects for future experiments.

II. EXPERIMENTAL PROCEDURES AND RESULTS

We have extracted yields of secondary fission fragments from measurements of the multiple γ rays emitted by different pairs of fragments formed in the spontaneous fission of ^{252}Cf. The experiment was carried out at the Holifield Heavy Ion Research Facility with the Oak Ridge Compton Suppression Spectrometer System. The 20 Compton suppressed Ge detectors were located at a source to detector distance of 14 cm. A hermetically sealed ^{252}Cf source with 6×10^4 spontaneous fission events per second was placed in the center of the detector array, and all the events of coincident γ rays with multiplicity $\geqslant 2$ were recorded. During a 5 day run approximately 2×10^9 γ-γ coincidences were collected event by event.

A two-dimensional matrix of γ-γ coincidences (4096×4096 channels) was created from the initial data by selecting the γ-ray coincidences occurring within 200 ns. The peaks seen in this two-dimensional spectrum arise from the coincidences between γ rays emitted (a) promptly by both complementary fission fragments of different fragment pairs, (b) promptly by one of the fragments in cascade, and (c) after the β decay of fission fragments. Only the peaks listed in (a) carry information on the yields of fission fragment pairs. We searched for γ-γ coincidence peaks and estimated peak areas by using the method suggested in [55]. The search was performed automatically using the special code FIT-2S created for this purpose [56]. In our approach, the full two-dimensional matrix was divided into different small regions, and each region was fitted with a complex two-dimensional function. This function is the sum of three terms. (1) The smooth background created by such γ-γ coincidences when both pulses originate from the incomplete absorption of the γ-ray energy. (2) Two series of ridges (parallel to the axes $E_{\gamma1}$ and $E_{\gamma2}$) originating from the coincidences of full absorption pulses with the pulses from the incomplete energy absorption of other γ rays. (3) Real peaks originating from coincidences of pairs of full absorption pulses. Examples of our two-dimensional γ-γ coincidence spectra are shown in Figs. 1(a)-(c) for three regions located around the coincidence peaks assocciated with $(2^+\rightarrow0^+)$ γ transitions for three selected pairs with 2, 8, and 10 neutron emission. The selected pairs are ^{106}Mo-^{144}Ba and ^{104}Mo-^{146}Ba [Fig. 1(a)], ^{104}Mo-^{140}Ba and ^{108}Mo-^{140}Ba [Fig. 1(b)], and ^{104}Mo-^{138}Ba [Fig. 1(c)].

The peak search and estimation took 8 h with an ALPHA computer for the whole 4096×4096 channel matrix. This procedure was repeated more than one time following shifts in the boundaries of the small regions to take care for the loss of peaks located near the region boundaries and to improve the smoothness of the background and background ridges at the boundaries of the small regions being used for fitting the total matrix. This procedure allows one to subtract background contributions, including ridges in both the X and Y directions. The table of data obtained in this way, including all the observed γ-γ coincidences, was used in the interpretation of the results. The list of real coincidence peaks, their assignments and areas are the final product of this procedure.

Along with the two-dimensional matrix, a number of one-dimensional spectra were built by using the events with three and higher fold coincidences of γ rays. These linear spectra were for γ rays detected in coincidence with two γ rays, with one emitted by each fragment of the pairs of interest, to confirm and check intensities of some weak γ transitions obtained from the γ-γ coincidence peaks.

Tables I–V present the independent yields of fission fragment pairs obtained for the five charge divisions of ^{252}Cf:

$$Z_L/Z_H = 46/52(\mathrm{Pd}-\mathrm{Te}),\ 44/54(\mathrm{Ru}-\mathrm{Xe}),$$

$$42/56(\mathrm{Mo}-\mathrm{Ba}),\ 40/58(\mathrm{Zr}-\mathrm{Ce}),\ 38/60(\mathrm{Sr}-\mathrm{Nd}).$$

For the pairs involving only even-even fragments, yields were determined from the areas of the peaks corresponding to coincidences between $2^+\rightarrow0^+$ transitions in both fragments. In the cases when odd A fragments occurred in the fragment pairs, all peaks involving γ transitions to their ground states were summed up to obtain the yields. For the nuclei of interest, we used the data on the low lying energy levels from Refs. [43,44,47,48,56–65].

Relative yields of fragment pairs were obtained after corrections for the known detection efficiencies and internal

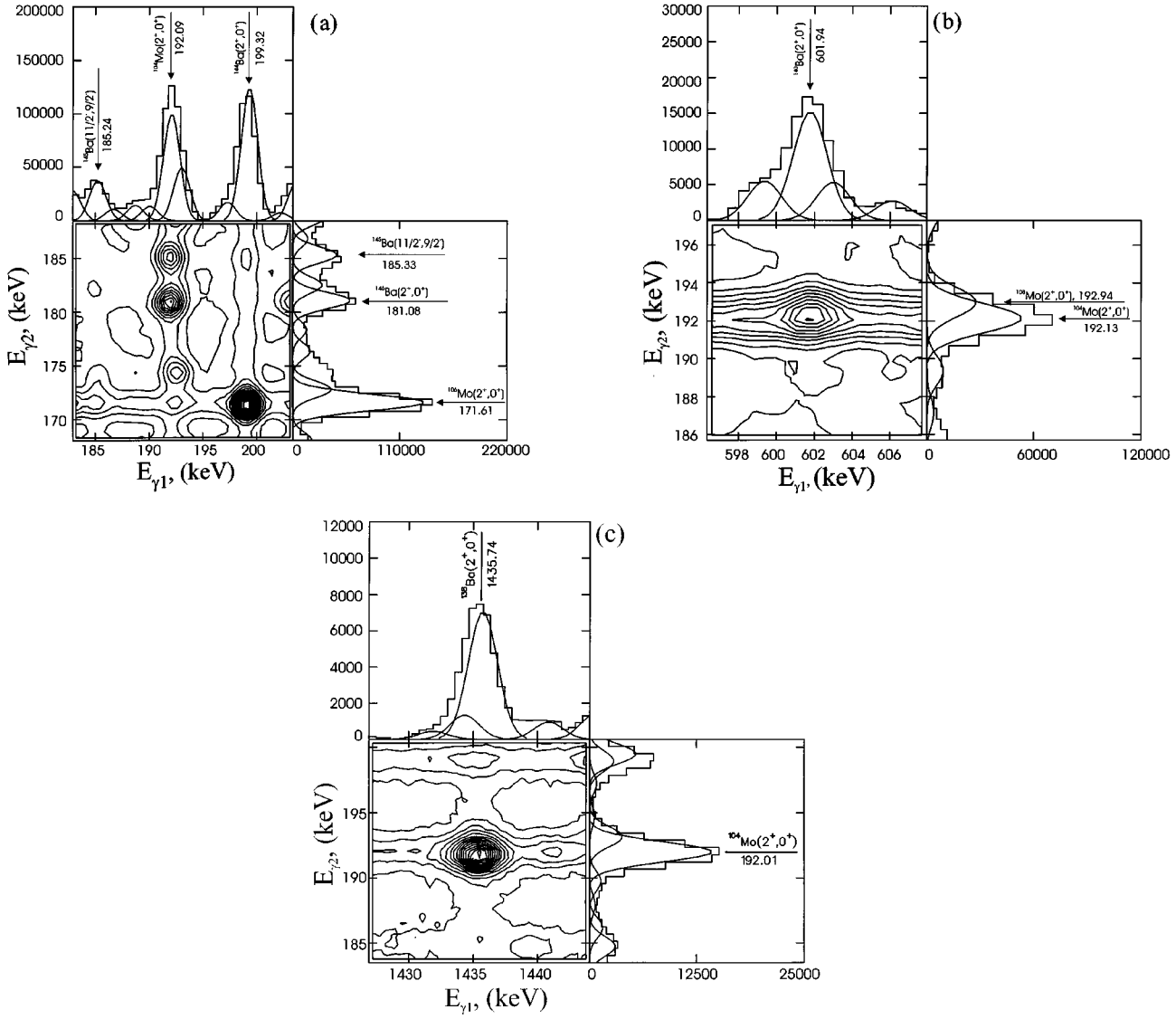

FIG. 1. Three examples of two-dimensional γ-γ coincidence spectra from different regions are shown. The contour lines represent equal count rates. Histograms in the upper and right panels show the projection spectra obtained after subtraction of the smooth background. Lines show the decomposition of these one-dimensional projection spectra into individual γ peaks. Besides the real coincidence peaks, ridges originating from the coincidences of full absorption pulses with the pulses associated with the incomplete energy release of the γ-ray energy are also seen. ''False'' peaks are also seen clearly at the intersections of some of the ridges. (a) Region of the peaks that are produced by coincidences of the $2^+ \rightarrow 0^+$ transitions in ^{106}Mo and ^{144}Ba and in ^{104}Mo and ^{146}Ba (two-neutron channels); this region also involves two peaks originating from coincidences of the $11/2^- \rightarrow 9/2^-$ transition in ^{145}Ba with the $2^+ \rightarrow 0^+$ transitions in ^{106}Mo (one-neutron channel) and ^{104}Mo (three-neutron channel). (b) Region involving coincidence peaks of the $2^+ \rightarrow 0^+$ transitions in ^{104}Mo and ^{140}Ba (eight-neutron channel). (c) Region involving coincidence peaks of the $2^+ \rightarrow 0^+$ transitions in the ^{104}Mo and ^{138}Ba (ten-neutron channel).

conversion probabilities. For those peaks involving ^{136}Xe a correction was made for the delay caused by the isomeric 2.9 μs $6^+ \rightarrow 4^+$ transition. For peaks that involved some odd mass fragments with high ground-state spins, corrections were made to take into account direct feeding of the ground states. Such corrections were important for ^{137}Xe and ^{139}Xe which have ground state spin 7/2. For ^{104}Mo and ^{138}Ba coincidence peaks between the 192.1 keV ($2^+ \rightarrow 0^+$) transition in ^{104}Mo and the 1435.8 keV ($2^+ \rightarrow 0^+$) and 462.8 keV ($4^+ \rightarrow 2^+$) transitions in ^{138}Ba were analyzed. The results were corrected for the contributions from the β decays of the ground state ^{138g}Cs ($T_{1/2}$=32.2 min) and isomeric state ^{138m}Cs ($T_{1/2}$=2.9 min), which also have a 192-462.8-

TABLE I. Yields of correlated fragment pairs of Pd-Te in the spontaneous fission of ^{252}Cf. Yields are given in percent, i.e., in number of pairs per 100 fission events. In the last line ($\overline{\nu}$) is the mean number of neutrons evaporated from the primary fragments.

	^{132}Te	^{134}Te	^{136}Te
^{108}Pd			0.02(2)
^{110}Pd			0.07(2)
^{112}Pd		0.08(2)	0.28(4)
^{114}Pd	0.03(2)	0.41(5)	0.18(3)
^{116}Pd	0.10(2)	0.11(2)	0.02(2)

TABLE II. Yields of correlated fragment pairs of Ru-Xe in the spontaneous fission of ^{252}Cf. Yields are given in percent, i.e., in number of pairs per 100 fission events. In the last line $(\overline{\nu})$ is the mean number of neutrons evaporated from the primary fragments.

	^{134}Xe	^{136}Xe	^{137}Xe	^{138}Xe	^{139}Xe	^{140}Xe	^{142}Xe
^{106}Ru					0.02(2)	0.08(2)	0.13(2)
^{107}Ru				0.05(5)	0.07(5)	0.19(5)	0.06(4)
^{108}Ru			0.02(1)	0.19(3)	0.23(2)	0.67(4)	0.12(3)
^{109}Ru		0.03(3)	0.08(4)	0.58(11)	0.30(7)	0.45(9)	0.05(5)
^{110}Ru		0.15(4)	0.30(4)	1.03(6)	0.58(4)	0.39(4)	0.02(2)
^{111}Ru		0.18(5)	0.22(4)	0.48(8)	0.26(6)	0.08(4)	
^{112}Ru	0.07(3)	0.20(5)	0.17(5)	0.24(3)	0.02(2)		
ΣY_{Xe}	0.07(3)	0.56(10)	0.79(10)	2.57(16)	1.48(11)	1.86(14)	0.36(8)
$\overline{\nu}$	6.0(2.6)	5.1(8)	4.4(6)	3.9(2)	3.5(2)	3.4(2)	2.3(2)

1453.8 keV coincidence cascade. For this correction we used data [66] on the level populations of ^{138}Ba following the β decay of the isomeric and ground states of ^{138}Cs and branching ratio of the isomeric state. Also, use was made of the relevant data known for the ^{252}Cf spontaneous fission: the cumulative yield of ^{138g}Cs (see Ref. [8]) and its isomeric ratio (see Ref. [67]). We estimated directly the count rate from the β decay of ^{138g}Cs by using the measured yields of γ-γ coincidence peaks of the pairs of γ transitions 1009.8 and 1435.8 keV, 547.0 and 1435.8 keV, 547.0 and 462.8 keV, 871.8 and 1435.8 keV, 409.0 and 1435.8 keV, 409.0 and 462.8, keV and of the 100% triple cascade of 191.96, 462.8 and 1435.8 keV. All these transitions occur between ^{138}Ba levels populated in the β decay of ^{138g}Cs. As a result of this correction, about one-half of the total yield of the 192.1–1435.8 keV coincidence peak (this total yield has about 1500 counts) has been found to be related to the β decays of ^{138g}Cs and ^{138m}Cs. The observed coincidence intensities of the 192.1 and 462.8 keV γ lines were explained as completely from the β decays of ^{138g}Cs and ^{138m}Cs.

The independent yields presented in Tables I–V are the result of normalization of the relative yields obtained in our experiment to the data for independent yields known from the literature for some particular fission fragments of ^{252}Cf (see Refs. [8,43]). One can see that for ^{138,140}Xe, ^{142,144,146}Ba, and ^{146,148}Ce all the pairs with large yields are present in Tables II–IV, e.g., all the Mo fragments connected to ^{144}Ba are present and so forth for other isotopes. Comparing these yields to relative total independent yields of these fragments measured in Refs. [8,43], we obtained the normalization factors which were used for calculations of the independent yields for all other observed pairs of Ru-Xe, Mo-Ba, and Zr-Ce (Tables II-IV). For the normalization of the data for the Pd-Te and Sr-Nd pairs (Tables I and V), the weighted mean of the normalization factors obtained for other pairs (Tables II–IV) was used. In Table VI we compare our values for the total yields of ^{138,140}Xe, ^{142,144,146}Ba, and ^{146,148}Ce (the relative yields specified above) with the known independent yields [43]. In the third column normalization factors, i.e., the ratios (R) of the numbers in the first and second columns, are given. The maximum deviation of the individual values of R from the weighted mean $[\langle R\rangle=(7.8\pm1.2)\times10^{9}]$ is 23%. Taking into account the errors quoted in Table VI, we regard as satisfactory the convergence of the individual normalization factors.

The obtained convergence of the normalization factors strongly supports the conclusion that the possible effect of the efficiency variation of the γ ray detector array with the

TABLE III. Yields of correlated fragment pairs of Mo-Ba in the spontaneous fission of ^{252}Cf. Yields are given in percent, i.e., in number of pairs per 100 fission events. In the last line $(\overline{\nu})$ is the mean number of neutrons evaporated from the primary fragments.

	^{138}Ba	^{140}Ba	^{141}Ba	^{142}Ba	^{143}Ba	^{144}Ba	^{145}Ba	^{146}Ba	^{147}Ba	^{148}Ba
^{102}Mo					0.02(2)	0.04(3)	0.09(6)	0.13(5)	0.10(7)	0.06(4)
^{103}Mo		0.05(3)	0.07(2)	0.02(2)	0.13(9)	0.67(10)	0.86(20)	0.46(8)	0.40(30)	0.12(9)
^{104}Mo	0.08(3)	0.18(4)	0.34(4)	0.36(4)	0.48(10)	1.14(4)	0.74(15)	0.39(4)	0.23(17)	0.04(3)
^{105}Mo	0.02(2)	0.07(5)	0.11(4)	0.65(10)	1.05(25)	1.30(11)	0.59(17)	0.13(7)	0.23(15)	
^{106}Mo	0.01(1)	0.12(3)	0.44(3)	0.92(4)	0.88(10)	0.65(4)	0.16(8)	0.08(5)		
^{107}Mo	0.02(2)	0.12(4)	0.11(3)	0.35(16)	0.14(8)	0.13(8)	0.15(7)			
^{108}Mo	0.02(1)	0.06(3)	0.10(3)	0.14(5)	0.12(10)	0.06(5)				
ΣY_{Ba}	0.15(6)	0.60(9)	1.17(10)	2.44(20)	2.82(29)	3.99(19)	2.58(32)	1.21(14)	0.96(37)	0.22(10)
$\overline{\nu}$	9.5(2.0)	6.5(1.0)	5.6(6)	4.3(4)	3.7(5)	3.4(2)	2.9(4)	2.3(3)	1.4(5)	1.1(5)

TABLE IV. Yields of correlated fragment pairs of Zr-Ce in the spontaneous fission of ^{252}Cf. Yields are given in percent, i.e., in number of pairs per 100 fission events. In the last line ($\overline{\nu}$) is the mean number of neutrons evaporated from the primary fragments.

	^{144}Ce	^{146}Ce	^{147}Ce	^{148}Ce	^{149}Ce	^{150}Ce
^{98}Zr		0.04(2)	0.02(2)	0.07(2)	0.08(4)	0.17(4)
^{99}Zr		0.04(4)		0.13(4)	0.26(14)	0.13(5)
^{100}Zr		0.11(3)	0.29(8)	0.63(5)	0.25(14)	0.29(5)
^{101}Zr	0.04(3)	0.47(9)	0.63(21)	0.62(16)	0.16(12)	0.06(3)
^{102}Zr	0.02(2)	0.41(5)	0.52(10)	0.44(5)	0.05(5)	0.03(3)
^{103}Zr	0.05(4)	0.15(5)	0.16(1)2	0.12(5)		
^{104}Zr		0.07(3)		0.05(5)		
ΣY_{Ce}	0.11(6)	1.29(13)	1.61(27)	2.06(19)	0.81(24)	0.68(15)
$\overline{\nu}$	5.9(2.9)	4.5(5)	3.7(6)	3.1(3)	3.2(9)	2.5(4)

value of mass and charge asymmetry of fission fragments is very small. In principle, one should anticipate some efficiency variation caused by the dependence of γ ray multiplicity on mass asymmetry. From the data of Ref. [7], we derived a value of 15% for the maximum possible variation of the efficiency within the range of mass and charge asymmetry covered by our data. This estimation is consistent with the results shown in Table VI. Since two neighboring isotopes at the peak of the yields have very similar multiplicities, this maximum 15% variation in efficiency applies only to the isotopes on the two wings of the distribution. In Tables I–V, the errors in the yields in the wings arise from data statistics, evaluations of internal conversion probabilities and correction factors specific to particular isotopes as discussed above and are already much larger then 15%. Thus this additional efficiency correction can be neglected.

To obtain information about the mean angular moments $\langle I_\gamma \rangle$, many additional γ-γ coincidence peaks involving transitions between different excited states of the fission fragments were analyzed. Relative transition intensities and level populations were derived for individual fragments when they appear together with different companions in the observed fragment pairs. The selection of such data associated with some Mo-Ba fragment pairs is presented in Table VII. The mean angular momentum values, as they follow from the observed level populations, will be discussed in Sec. III D in terms of their correlation with the primary fragment excitation energy.

III. DISCUSSION

The new individual yields (Tables I-V), neutron multiplicities (Fig. 1), and spin populations (Table VII) for correlated pairs are significant extensions of the known spontaneous fission characteristics. The older integral data correlate well with our new detailed results as presented in the next four subsections.

TABLE V. Yields of correlated fragment pairs of Sr-Nd in the spontaneous fission of ^{252}Cf. Yields are given in percent, i.e., in number of pairs per 100 fission events. In the last line ($\overline{\nu}$) is the mean numbers of neutrons evaporated from the primary fragments.

	^{150}Nd	^{152}Nd	^{154}Nd
^{96}Sr	0.03(2)	0.26(12)	0.23(11)
^{98}Sr	0.05(2)	0.32(16)	

TABLE VI. Normalization factors.

Fission fragments	Relative yields $\times 10^6$	Independent yields [53] (%)	Normalization factors (R) $\times 10^8$
^{138}Xe	192(7)	2.30(34)	83(13)
^{140}Xe	123(8)	1.50(22)	82(13)
^{142}Ba	174(10)	2.90(43)	60(10)
^{144}Ba	306(12)	3.60(54)	85(13)
^{146}Ba	94(8)	1.01(15)	92(16)
^{146}Ce	88(6)	1.04(16)	84(14)
^{148}Ce	140(11)	2.31(34)	61(10)

A. Independent yields of fission fragments

Previously obtained data on mass and charge distributions of fission fragments correspond to more integral fission characteristics in contrast to the new detailed results of our work. However, some of these integral characteristics can be deduced from our results. In the next to last lines of Tables II–IV, the independent yields are given for some fission fragments. These are sums of the yields of the individual fragment pairs presented in the corresponding columns. Independent yields for some fragment pairs not listed in Tables I–V (often because the decay schemes are not known), were estimated after two-dimensional B spline interpolations[2] of the data. Uncertainties introduced by these interpolations which depended on the results of these procedures are included in the errors given for the data and are discussed later. Our integral independent yields are displayed in Fig. 2 and are in general agreement with the data of Ref. [43]. For a number of fragments these include values which were not known before. Total integral yields of fission fragments of different nuclear charges, that emerge from our results, are presented in the second column of Table VIII. Similar integral data reported by other authors are presented in the following three columns of this table.

B. Neutron multiplicity distributions

The results presented in this paper are mostly the new type of data which could not be obtained before with conventional methods. All previous information on the prompt neutron multiplicity distributions at low-energy fission has been obtained from measurements involving neutron detection. In this standard approach, extraction of neutron multiplicity distributions requires assumptions about the shape of these distributions and the neutron detector response function, and a complex unfolding of the experimental data (see

[2]See Ref. [73] and Ref. [74].

TABLE VII. Relative intensities of γ transitions between the levels of the ground-state bands in some Mo and Ba fragments. Intensities of the $2^+ \rightarrow 0^+$ transitions are assumed to be equal 1.0 for normalization. Also presented are the mean angular momenta $\langle I_\gamma \rangle$ derived from the obtained population of all excited states of the fragments and the mean numbers of neutrons ($\overline{\nu}$) evaporated from the primary fragments, obtained from the unfolding procedure described in Sec. III C.

		Relative transition intensities					
Fragment	Partner	$4^+ \rightarrow 2^+$	$6^+ \rightarrow 4^+$	$8^+ \rightarrow 6^+$	$10^+ \rightarrow 8^+$	$\langle I_\gamma \rangle$	$\overline{\nu}$
^{104}Mo	^{147}Ba	0.90(19)	0.54(19)			4.9(12)	0.18(2)
^{104}Mo	^{146}Ba	0.69(4)	0.47(4)	0.15(6)		4.6(7)	0.84(2)
^{104}Mo	^{145}Ba	0.71(4)	0.41(2)	0.14(2)	0.06(30)	4.5(3)	1.30(4)
^{104}Mo	^{144}Ba	0.72(3)	0.41(3)	0.08(1)		4.4(3)	1.66(5)
^{104}Mo	^{143}Ba	0.80(6)	0.32(5)	0.20(1)		4.5(6)	2.11(10)
^{104}Mo	^{142}Ba	0.43(7)	0.31(5)	0.17(5)		3.8(7)	2.46(15)
^{104}Mo	^{140}Ba	0.29(9)	0.21(12)			3.0(10)	3(1)
^{104}Mo	^{138}Ba	<0.2				2.2(4)	3 (1)
^{146}Ba	^{104}Mo	0.82(7)	0.41(4)	0.22(8)	0.22(9)	8.2(14)	1.11(2)
^{144}Ba	^{104}Mo	0.92(3)	0.64(4)	0.50(4)	0.07(1)	7.2(10)	2.30(5)
^{142}Ba	^{104}Mo	0.96(8)	0.35(3)			4.8(7)	3.54(15)
^{140}Ba	^{104}Mo	0.99(9)	0.21(8)			4.4(3)	5(1)
^{138}Ba	^{104}Mo	<0.2				2.2(4)	7(1)
^{144}Ba	^{106}Mo	0.93(5)	0.82(5)	0.49(5)		7.8(15)	1.00(5)
^{144}Ba	^{105}Mo	0.80(9)	0.60(6)	0.41(2)		8.0(10)	2.10(5)

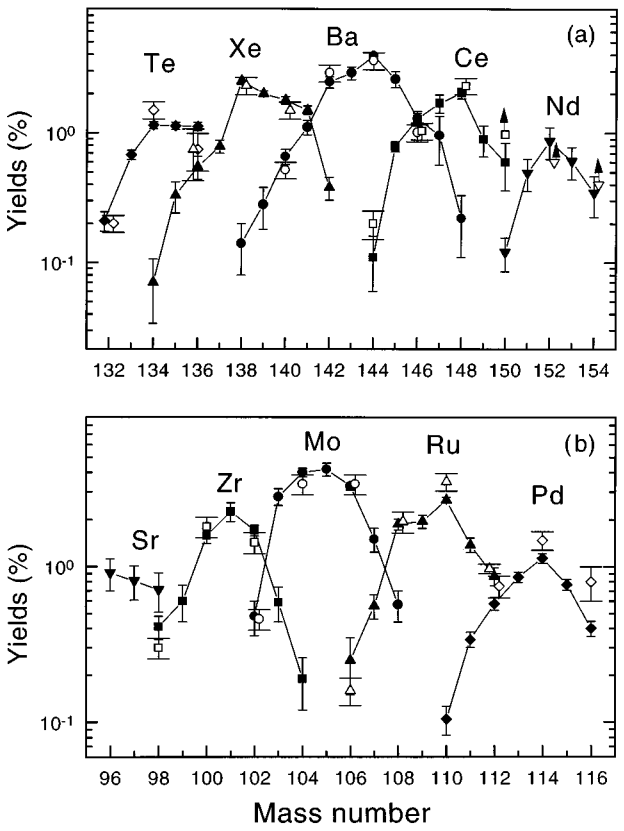

FIG. 2. Summary of fission fragment isotopic distributions deduced from the fragment pair independent yields given in Tables I–V (closed symbols) are presented. The yields are presented in percents to the total number of fission events. For comparison the data of Ref. [43] are shown (open symbols).

Refs. [69–71], for example) and of course, zero neutron emission is not detected. Only the total neutron distributions have been obtained from these complex analyses. More sophisticated measurements (see, for example, Refs. [25,27,72]) allowed one to deduce the variation of the mean neutron numbers ($\overline{\nu}$) of individual fragments and variances (σ_ν) with fission fragment mass.

Here we report the direct measurements of neutron multiplicities. Figure 3 shows the more complete prompt neutron multiplicity distributions obtained from Tables I–V for different charge splits of ^{252}Cf. These results extend our earlier reported distributions [1,2,47–50]. In Fig. 4 the sum of the neutron multiplicity distributions from Tables I-V for each neutron evaporation number shown in Fig. 3 is compared with the total neutron multiplicity distribution for ^{252}Cf known from literature [68]. We note that the even-Z–even-Z charge divisions in our data points in Fig. 4 account for more than 40% of the total ^{252}Cf spontaneous fission (see the second column of Table VIII). The odd-Z–odd-Z nuclei correspond to about 50% of the yields.

The lower values for our data in Fig. 4 for the multiplicities ranging from two through six, as compared to the data of Ref. [68], are related to the fact that in our data we observed only a part of the fission events. An excess of zero neutron events in our data over the data of Ref. [68] shows that the neutron detection method employed in Ref. [68] (and in other similar papers) probably underestimates yields of zero neutron events. The agreement (within the error bars) of our data and the data of Ref. [68] for the multiplicities of $\geqslant 7$ shows that the major part of these high multiplicity events comes only with a few charge divisions as shown in our data.

From our data we find that when $\geqslant 7$ neutrons are evaporated from the fission fragments nearly all of these fission events occur in the Mo-Ba split of ^{252}Cf. In the last lines of

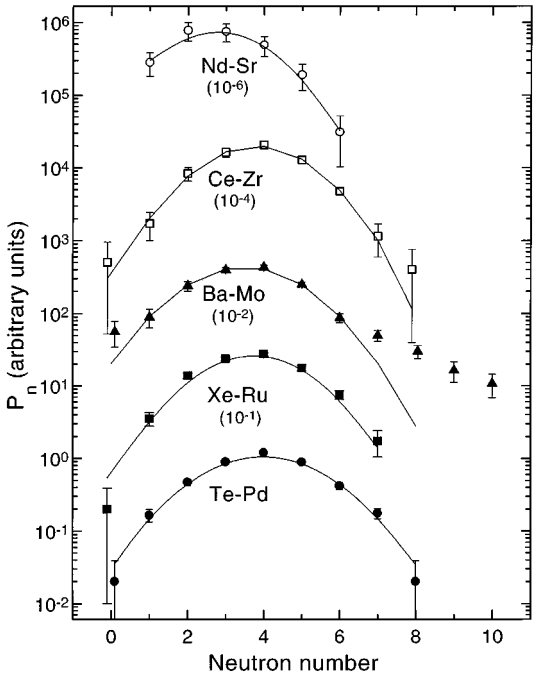

FIG. 3. Multiplicity distributions of prompt neutrons deduced from Tables I–V for different charge splits are shown. The P_n values (relative yields P_n) multiplied by the factors given below each correlated fragment charge pair gives the yield values in percents to the total number of fission events. The curves show simple Gaussian fits to the data (see text).

Tables II–IV are shown the mean numbers of neutrons emitted when a particular fragment (e.g., ^{142}Ba, etc.) was formed.

All neutron multiplicity distributions shown in Fig. 3 except the Mo-Ba distribution could be well fitted with Gaussian curves. However, the Mo-Ba distribution could not be approximated by any single Gaussian because of the excess of 7–10 and zero neutron events. Excluding these points, we could also fit the Mo-Ba data with a single Gaussian. The single Gaussian fits are also shown in Fig. 3. In Table VIII (columns 6 and 7) the mean neutron multiplicity ($\overline{\nu}_{\rm expt}$) and their variances ($\sigma_{\rm expt}$), derived from the experimental points shown in Fig. 3, are displayed, together with the mean numbers of prompt neutrons given by Nifenecker *et al.* [7] (see the last column). Among the neutron multiplicity distributions shown in Fig. 3, the distribution associated with the Mo-Ba charge division is notable for enhancements of the lower (0) and higher (7–10) neutron multiplicities. Noteworthy is the observation of the ^{104}Mo-^{138}Ba pair appearing as a result of the ^{252}Cf spontaneous fission event associated with the evaporation of 10 neutrons (see Table III). The split ^{104}Mo-^{138}Ba with 10 neutron emission is clearly seen in Fig. 1(c). This is an observation of 10 neutron emission in spontaneous fission. Our results with zero neutron emission are consistent with the findings made for the ''cold compact fragmentation'' (see Refs. [39,40,71]) with respect to the fragment mass and charge asymmetry where zero neutron pairs are obtained and from the point of view of yields of these pairs. The observed zero neutron pairs were discussed in our earlier papers [75,76] in terms of the phenomenon of cluster radioactivity.

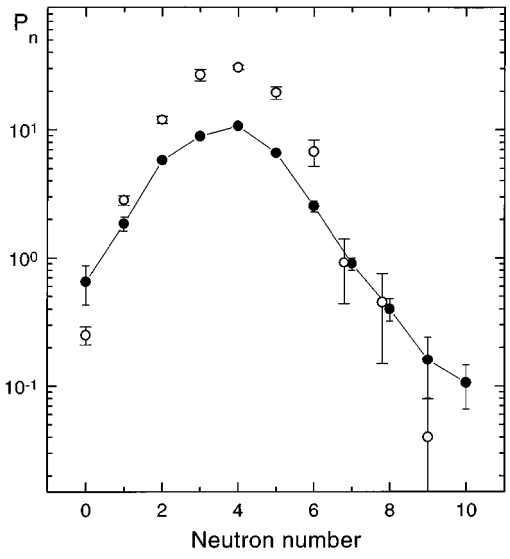

FIG. 4. Summed neutron multiplicity distribution (solid circles), where the summing is made over five investigated charge divisions presented in Fig. 3. This distribution corresponds to only about 41.8% of the total number of spontaneous fission events of ^{252}Cf (see Table VIII). The total neutron multiplicity distribution from Ref. [68] normalized to 100% is shown for comparison (open circles).

C. Mass and excitation energy distributions of primary fragments

The fragment pair experimental yields obtained in this work originate from deexcitation of primary fission fragments, and carry information about the mass and excitation energy distributions of the primary fission fragments of fixed charge splits $Y(A_L,E_L^*,A_H,E_H^*|Z_L,Z_H)$. Two possible ways to use such data are the following. One is to test the ability of different theories to predict the primary fragment distributions which reproduce the experimental data after applying a statistical code for modeling the deexcitation of primary fragments. A second way is to extract the primary fragment distributions by unfolding the experimental data.

The numbers given in Tables I–V are the experimental yields $Y^{\rm expt}(A_L^{'},A_H^{'}|Z_L,Z_H)$ of secondary fission fragment pairs created after neutron evaporation. One can connect these yields to the yields of primary fission fragment pairs $Y(A_L,A_H|Z_L,Z_H)$ by the following equations:

$$Y^{\rm calc}(A_L^{\prime},A_H^{\prime}|Z_L,Z_H)=\sum_m \sum_{(A_L,A_H)} Y(A_L,A_H|Z_L,Z_H) \times I_L \times I_H, \tag{2}$$

$$I_L=\int F(E_L^*,A_L)\times P_n(E_L^*,A_L)\times \delta(A_L-A_L^{'}-n)dE, \tag{3}$$

$$I_H=\int F(E_H^*,A_H)\times P_n(E_H^*,A_H)\times \delta(A_H-A_H^{'}-n)dE, \tag{4}$$

where $F(E^*,A)$ is the excitation energy distribution of each primary fission fragment, $P_n(E^*,A)$ is the probability of

TABLE VIII. Total integral yields for different charge splits and corresponding neutron multiplicities ($\overline{\nu}$) and their variances (σ_ν) again. Results from this work and from previous references are shown for comparison (see also text of Sec. III B).

Charge split	Yield (%) This work	[70]	[8]	[65]	$\overline{\nu_{\rm tot}}$ This work	σ_ν This work	$\overline{\nu_{\rm tot}}$ [7]
Pd-Te [a]	4.3(4)	7.8(3)	7.3	9.4(1.0)	4.0(3)	1.4(3)	3.9(1)
Ru-Xe	9.7(3)	13.6(2)	13.5	16.5(5)	3.77(12)	1.3(2)	3.9(1)
Mo-Ba	17.2(7)	15.3(3)	16.3	18.5(5)	3.72(25)	1.85(37)	3.6(1)
Zr-Ce	8.2(5)	7.9(3)	8.7	9.4(5)	3.65(21)	1.46(15)	3.5(1)
Sr-Nd [a]	2.4(4)	2.90(15)	3.4	2.5(5)	2.9(9) [b]	1.5(5)	3.7(3)

[a]For Pd-Te and Sr-Nd pairs the yields of fragment pairs (see Tables I–V) as shown, include only a limited number of pairs, often because the decay schemes are not known. The two-dimensional *B* splin interpolation is applied to include some missing pairs and to obtain the total integral yields presented in this table. The additional inaccuracies introduced by *B* spline interpolation are included to the errors presented here.

[b]This number presumably is low because only a few low neutron multiplicity fragment pairs were analyzed. The error was increased to include this.

evaporation of n neutrons from a primary fragment ($n=A-A'$). Equation (2) involves two summations: the first one is done over all primary fragment pairs (A_L, A_H) of a given charge split, and the second is introduced to take into account possible contributions of more than one fission mode.

The unfolding procedure is based on the least squares method and implied minimization of the form

$$\chi^2=\frac{1}{N_{\rm expt}-N_{\rm par}} \times\sum\left[\frac{Y^{\rm expt}(A_L',A_H'|Z_L,Z_H)-Y^{\rm calc}(A_L',A_H'|Z_L,Z_H)}{\sigma_{\rm expt}(A_L',A_H'|Z_L,Z_H)}\right]^2, \tag{5}$$

where, separately for each charge split, the summation is done over all the fragment pairs of a fixed charge division for which the yields were obtained in the experiment. In the fitting procedures [Eq. (5)] the following parameters were varied. The mean value of the fragment total kinetic energy, $\langle$TKE$\rangle$, variance of the total kinetic energy, $\sigma_{\rm TKE}$, the mean mass value of heavy primary fragments, $\langle A_H\rangle$, variance of this mass, σ_{A_H}, and mean values of the excitation energy of heavy primary fragments, $\langle E_H^*\rangle$.

To make the task feasible we assumed that the primary fragment mass and excitation energy distributions can be described by simple forms with a small number of parameters. Separately for each charge split the minimum values of χ^2 were searched by varying these free parameters. The outlined procedure could be applied only if extensive data for the yields of secondary fission fragment pairs of the same charge split are known, and some hypotheses about the distributions searched are made. In the data presented here three charge divisions Xe-Ru, Mo-Ba, and Zr-Ce (Tables II–IV) are notable for their extensive data. For each of these charge splits, we unfolded the distributions of $Y(A_L,E_L^*,A_H,E_H^*|Z_L,Z_H)$.

Best fits of the calculated yields $Y^{\rm calc}(A_L',A_H'|Z_L,Z_H)$ to the yield patterns given in Tables II–IV were obtained by assuming Gaussian forms for the mass and excitation energy distributions of the primary fission fragments of a fixed fission mode. Also the following two additional assumptions were made in order to reduce the total number of free model parameters.

(1) First we assumed that, for a particular charge split and at a fixed fission mode, the mean value of the total kinetic energy $\langle$TKE$\rangle$ and its variance $\sigma_{\rm TKE}$ are the same for different primary fragment pairs. These assumption and the following relations between the parameters of our model

$$Q_{\rm fiss}=\langle{\rm TKE}\rangle+\langle E_L^*\rangle+\langle E_H^*\rangle, \tag{6}$$

$$\sigma_{\rm TKE}^2=\sigma_{E_L^*}^2+\sigma_{E_H^*}^2, \tag{7}$$

allowed us to reduce the number of free parameters. Here $\langle E_{L(H)}^*\rangle$ and $\sigma_{E_{L(H)}^*}$ are the fragment mean excitation energy values and their variances. Equation (6) follows from Eq. (1), and both Eqs. (6) and (7) are valid in the framework of the model underlying Eq. (2) and an assumption of the Gaussian form for the primary fragment excitation energy distribution.

(2) Second we impose the additional boundary conditions

$$\frac{\sigma_{E_H^*}^2}{\langle E_H^*\rangle}=\frac{\sigma_{E_L^*}^2}{\langle E_L^*\rangle} \tag{8}$$

between the dispersions of the energies of the light and heavy fragments as defined above.

For each charge split, the mean excitation energies $\langle E_H^*\rangle$ were searched for nine heavy primary fragments centered around the mean mass fragment. Deexcitations of primary fission fragments were calculated by employing the statistical code GNASH [77]. The reliability of the results obtained with the code was confirmed by test calculations of (α,xn) fusion-evaporation reactions studied in different experiments [78–81].

At first it appeared ''natural'' to carry out the outlined unfolding procedures by assuming that only a single fission mode contributes to each of the yield patterns given in Tables II-IV. In fact, taking only one fission mode (referred to later as mode 1), we successfully fitted the data for the Ru-Xe and Zr-Ce fragment pairs given in Tables II and IV as seen in Fig. 3. However, no reasonable solution could be

TABLE IX. Excitation energies of primary fragments in mode 1.

A_{Ba}	$\langle E^*_{Ba}\rangle$ (MeV)	$\sigma_{E^*_{Ba}}$	A_{Mo}	$\langle E^*_{Mo}\rangle$ (MeV)	$\sigma_{E^*_{Mo}}$
148	16.5(11)	8.4	104	8.4(6)	4.3
147	21.3(3)	9.3	105	4.3(1)	1.9
146	11.8(7)	5.6	106	16.3(10)	7.7
145	16.6(8)	8.0	107	10.6(5)	5.1
144	9.7(6)	4.2	108	19.5(12)	8.4
143	13.7(5)	6.6	109	13.9(5)	6.7

obtained with any single fission mode for the pattern of the Mo-Ba yields. This was to be expected because the Mo/Ba split has strongly enchanced high neutron multiplicity yields (see Fig. 3) that are not seen in the charge divisions of Ru/Xe (44/54) and Zr/Ce (40/58) that occur to either side of Mo/Ba (42/56). In fact, the majority of the 7 and 8 neutrons and all of the 9 to 10 neutron yields are in the Mo/Ba split. These high neutron multiplicity events must be going via a different mode than (a) the standard mode described by a single Gaussian fit to the distributions to either side of Mo/Ba and (b) the standard mode which describes by a similar single Gaussian fit the 1–5 neutron high intensity yields of the Mo/Ba. Thus, the second mode is needed to fit the high neutron multiplicity data. An excellent fit to the data of Table III was obtained by assuming that *two distinct fission modes* (mode 1 and mode 2) contribute to the formation of the primary Mo-Ba fission fragments. Actually, this implies that their mass distribution is a superposition of two Gaussians, and their excitation energy distributions are also mixtures of two Gaussians. Characteristics of these two fission modes for Mo-Ba charge split extracted from the above calculations are presented below and in Tables IX and X.

Mode 1:

$$\langle \mathrm{TKE}\rangle = 189 \pm 1 \ \ \mathrm{MeV},$$

$$\sigma_{\mathrm{TKE}} = 9.43 \pm 0.11 \ \ \mathrm{MeV},$$

$$\overline{A_H} = 145.7 \pm 0.1, \quad \overline{A_L} = 106.3 \pm 0.1,$$

$$\sigma_{A_H} = \sigma_{A_L} = 2.02 \pm 0.13.$$

Mode 2:

$$\langle \mathrm{TKE}\rangle = 153 \pm 4 \ \ \mathrm{MeV},$$

$$\sigma_{\mathrm{TKE}} = 12.5 \pm 3.2 \ \ \mathrm{MeV}.$$

The intensity ratio of the two modes:

$$\text{Total: } I_1/I_2 = 14.$$

TABLE X. Excitation energies of the only three primary fragments pairs in mode 2. One or all of them can contribute to the second fission mode.

A_{Ba}	$\langle E^*_{Ba}\rangle$ (MeV)	$\sigma_{E^*_{Ba}}$	A_{Mo}	$\langle E^*_{Mo}\rangle$ (MeV)	$\sigma_{E^*_{Mo}}$
146	45.0(37)	12.9	106	16.9(14)	4.8
145	39.7(26)	10.4	107	23.8(16)	6.2
144	35.4(26)	8.0	108	33.2(24)	7.5

In the above characteristics of fission modes and in Tables IX and X the meaning of the used values follows: $\langle E^*_{Ba}\rangle$ and $\langle E^*_{Mo}\rangle$ are average excitation energies for each fragment (A_{Ba}, A_{Mo}) and $\sigma_{E^*_{Mo}}$ are their variances. Also $\langle \mathrm{TKE}\rangle$ is the average total kinetic energy, σ_{TKE} is its variance, $\overline{A_H}$ and $\overline{A_L}$ are average high and low fragment masses, and σ_{A_H}, σ_{A_L} are their variances.

In principle, one can ask whether the yield pattern of the Mo-Ba fission fragments presented in Table III could be fitted with an assumption of an asymmetric TKE distribution. However, in this case one would obtain, for the primary fragments, TKE and E^*_H (E^*_L) distributions which have considerable tails not seen in any other charge splits. We excluded this possibility because it is natural to assume that the only fission mode (with Gaussian TKE and E^*_H (E^*_L) distributions) revealed in the Ru-Xe and Zr-Ce splits also dominates in the Mo-Ba split. In addition the Mo/Ba 6–10 neutron multiplicity distribution data are not characteristic of a smoothly decreasing asymetric tail. A second mode with a Gaussian distribution is also in line with the generally adopted position of ''Gaussian-like'' TKE and excitation energy distributions of fission fragments (Ref. [24]).

As one can see in Table IX, mode 1 looks like the familiar fission mode of ^{252}Cf, and its principal characteristics ($\langle \mathrm{TKE}\rangle, \sigma_{\mathrm{TKE}}, A_{H(L)}$) are very close to those that were known before (Ref. [25]). Our value of $\sigma_{\mathrm{TKE}} = 9.43$ MeV is somewhat lower compared to the value reported [25] for the mass asymmetry 146/106, but this difference looks to be reasonable taking into account that fragments of various charge splits contribute to the same mass split. Also, excitation energies of the primary fragments given for this mode in Tables IX and X fit the mean neutron multiplicity for the ^{252}Cf fragments of these mass numbers [25]. The characteristics of mode 1 obtained for the Mo-Ba split are compared in Tables XI and XII with those obtained for single fission modes fitting the yields of Ru-Xe and Zr-Ce fragment pairs. Mode 1 results for these three charge splits are seen to be very similar as expected. This also involves the reasonable tendency obtained for the $\langle \mathrm{TKE}\rangle$ variation with the charge asymmetry of the fission fragments (see Tables XI and XII).

Mode 2 obtained for the Mo-Ba split appears quite unusual because of its quite low value of $\langle \mathrm{TKE}\rangle$ and very narrow mass distribution compared to mode 1 (see Tables IX and X). Actually, good fits to the data of Table III were

TABLE XI. Total characteristics of the fission mode 1 at scission for three charge divisions: Ru-Xe, Mo-Ba, and Zr-Ce, derived from fits to the yields of fission fragment pairs. $\langle A_H\rangle$ and σ_H stand for the mean mass of the heavy primary fragments and variances of the primary fragment mass distributions.

Charge split	Ru/Xe	Mo/Ba	Zr/Ce
χ^2	1.07	0.89	0.98
$\langle \mathrm{TKE}\rangle$	193.3(3)	189.3(1)	183.3(3)
σ^2_{TKE}	95(7)	89.5(4)	99(9)
$\langle A_H\rangle$	139.7(3)	145.7(1)	150.1(2)
σ_A	2.6(1)	2.0(1)	1.9(1)

TABLE XII. Total characteristics of the fission mode 1 for three charge divisions: Ru-Xe, Mo-Ba, and Zr-Ce. Excitation energies of heavy primary fragments.

	Fragment excitation energies (MeV)		
Mass number	Xe	Ba	Ce
138	22.9(8)		
139	5(1)		
140	19(1)		
141	6.6(3)		
142	22.0(7)	23(1)	
143	17(1)	13.7(5)	
144	11(2)	9.7(5)	
145	11(3)	16.6(2)	
146		11.8(6)	
147		21.3(2)	17(2)
148		16.5(8)	5.5(6)
149		24(3)	17.3(4)
150		18(4)	21.8(5)
151			19.9(1)
152			17(1)
153			10(3)

found by searching for the optimal set of the parameters $\langle \mathrm{TKE} \rangle$, σ_{TKE}, A_H, σ_{A_H}, and E^*_{Hj} for the fission mode 1, when only one Mo-Ba primary fragment pair contributes to mode 2. So, only $\langle \mathrm{TKE} \rangle, \sigma_{\mathrm{TKE}}$, and E^*_H were searched for in mode 2. Very reasonable fits were found when the single primary fragment pair responsible for mode 2 is ^{106}Mo-^{146}Ba, ^{107}Mo-^{145}Ba, or ^{108}Mo-^{144}Ba. For 16 varied parameters and 32 free points, χ^2 values of 0.85, 0.89, and 0.92 were obtained for these pairs, respectively. Each of these fragment pairs had essentially the same $\langle \mathrm{TKE} \rangle = 153 \pm 3$ MeV in mode 2. Parameters of mode 1 were independent of the choice of the pair contributing to mode 2. The ^{106}Mo-^{146}Ba pair gives the best fit to the data of Table III which relate, in particular, to the Mo-Ba pairs corresponding to emission of 7–10 neutrons (see Fig. 7 shown later). However, the data do not unambiguously determine which of the three primary fragment pairs or their combinations are responsible for the existence of mode 2.

The very low $\langle \mathrm{TKE} \rangle$ value for the fission mode 2 emerges because this mode is responsible for the yields of the lightest Mo-Ba pairs which involve emission of the highest numbers of neutrons (7–10). This large difference in $\langle \mathrm{TKE} \rangle$ between modes 1 and 2 is directly connected with the enormous excitation energy of the primary fragments in mode 2 where neutron evaporation is much higher. Our fits show that the excitation energy is unequally divided between two fragments for the primary fragment pairs of ^{106}Mo-^{146}Ba and ^{107}Mo-^{145}Ba. This conclusion of an unequal split of energy does not depend on the model but is driven by the experimental data as shown in Table III. As seen in Table III, and when compared to Tables II and IV, only for the barium fragments does one definitely see a mass variation of 11 units as seen in coincidence with ^{104}Mo (^{148}Ba-^{138}Ba). For its Mo partners the observable masses are distributed over only seven mass units, and the maximum number definitely seen in coincidence with any Ba isotope is six for ^{143}Ba. Since the starting points after fission are the zero neutron channels peaked around ^{107}Mo-^{145}Ba to ^{104}Mo-^{148}Ba and, after neutron evaporation the lowest mass ending points are $^{102-104}$Mo and $^{138-140}$Ba, these data clearly indicate that most of the neutrons in the high neutron emission events come out of the Ba fragments – not the Mo fragments. Thus the Ba fragment in mode 2 must have larger excitation energy to evaporate 6–8 neutrons compared to 1–4 evaporated from the Mo fragment. Our fits that give the Ba fragments the larger excitation energy in mode 2 thus are in agreement with the conclusion one extracts directly from the experimental data. It is especially high for the heavy fragment ^{146}Ba, whereas its partner, ^{106}Mo, bears a quite ''normal'' excitation. The situation looks similar for the ^{107}Mo-^{145}Ba pair. In the case of the ^{108}Mo-^{144}Ba pair, the excitation of ^{108}Mo approaches that for ^{144}Ba, and both fragments, ^{144}Ba and ^{108}Mo, have an excitation energy considerably higher than the excitation energy of these fragments in fission mode 1.

Assuming that the barium fragments are cold at scission and have the form of symmetrical spheroids and using the simple formula of Ref. [24] derived from the liquid drop model, we estimated the ratios of the long to short axes at scission to be $a/b = 3.2$, 3.0, and 2.8 for ^{146}Ba, ^{145}Ba, and ^{144}Ba, respectively. The distances between the fragment charge centers at the scission point that follow from these axis ratios correspond well to the low $\langle \mathrm{TKE} \rangle$ value of mode 2 (153 MeV). This correspondence follows from the considerations made on the basis of the scission point model [30]. Of course, it is an upper limit to assume that the whole excitation energy obtained at scission is stored in fragment deformation. To go further an upper limit of 10 MeV was estimated for the thermal excitation of ^{252}Cf at scission [35–37]. Even with this conclusion, in the most likely charge split in mode 2, ^{106}Mo-^{146}Ba the ^{146}Ba has a 3:1 axes ratio and the less favored cases have only somewhat smaller ratios of 2.8 and 2.6. Thus, one or all three of these Ba isotopes are hyperdeformed in mode 2 at scission. This is the first definite evidence for hyperdeformed nuclear shapes briefly reported earlier in Refs. [2,47,48,50]. It is possible that some reasonable modifications of the hypotheses underlying our unfolding procedure might change somewhat the numerical results given in Tables X and XI. However, we believe that the data will necessarily lead to the conclusion that two distinct modes occur in the Mo-Ba fission of the ^{252}Cf nucleus. Our conclusion made about the unusually high excitation energy of the Ba fragments in the case of the second mode comes quite independent of the details of these hypotheses.

The excitation energy spectrum of ^{146}Ba is shown in Fig. 5 (curve 1). This spectrum follows from the unfolding of the data of Table III when ^{146}Ba is assumed to be responsible for the fission mode 2. In this figure curve 2 shows the calculated mean number of evaporated neutrons as a function of the excitation energy of ^{146}Ba and demonstrates that this fragment should have an excitation energy of up to about 70 (60) MeV in order to produce the secondary fragment ^{138}Ba (^{140}Ba) through the evaporation of eight (six) neutrons. The complementary fragment ^{106}Mo gives the secondary fragment ^{104}Mo as a result of evaporation of two neutrons. The excitation energy spectrum of ^{146}Ba (Fig. 5)

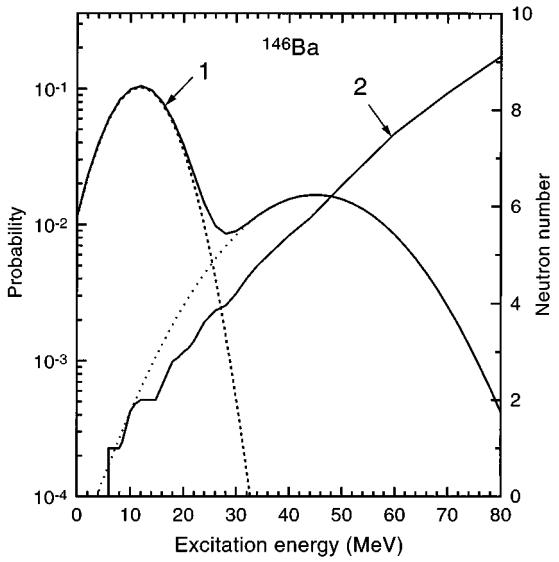

FIG. 5. Excitation energy spectrum (curve 1, solid, left scale) and mean number of evaporated neutrons (curve 2) vs the excitation energy of ^{146}Ba fragment. It is assumed that two fission modes are present, and only the primary fragment pair ^{106}Mo-^{146}Ba contributes to the second fission mode. The contributions of the first and second fission modes to the excitation energy spectrum are shown with dashed curves (see also text in Sec. III C).

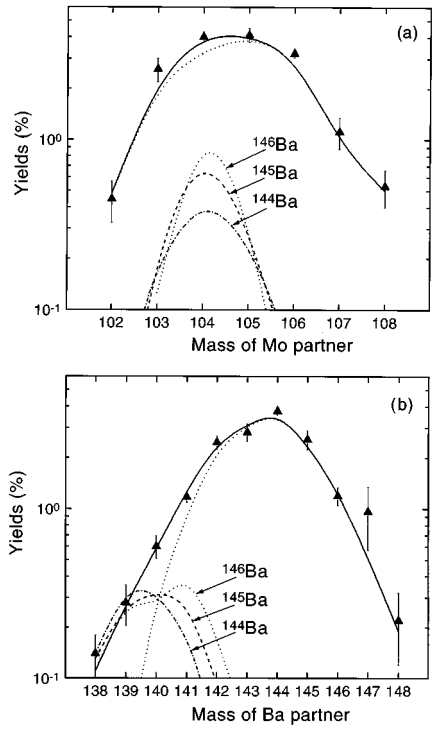

FIG. 6. (a) and (b) Results of the unfolding procedures for the Mo and Ba fragment isotopic distributions (solid curve) are compared to our experimental (triangles) total fission fragment isotopic distributions (see also Fig. 2). Dotted curves show the contributions of the first and second fission modes, assuming that the ^{106}Mo-^{146}Ba primary fragment pair is responsible for the second fission mode. The dashed and dash-dotted curves show, alternative contributions to the second fission mode by the ^{107}Mo-^{145}Ba and ^{108}Mo-^{144}Ba primary fragment pairs, respectively (see also text in Sec. III C).

demonstrates the distinct character of two fission modes. In order to fit the yield pattern of Table III, this spectrum must be a composition of two Gaussians and not a single Gaussian folded with a high-energy tail. These observations remain valid also if ^{108}Mo-^{145}Ba and/or ^{107}Mo-^{145}Ba are responsible for mode 2. Figures 6 and 7 show the results of the discussed unfolding procedure from the point of view of how it fits the experimental mass (Fig. 6) and neutron multiplicity (Fig. 7) distributions obtained for the Mo-Ba split of ^{252}Cf.

For the Mo-Ba split the intensity of mode 2 was estimated in relation to the strength of mode 1 as $I_2/I_1 = 1/14$. For the Ru-Xe and Zr-Ce splits we estimated the upper limits of such a ratio, as $\leqslant 1/90$ and $\leqslant 1/40$, respectively (see Tables IX and X). The limit for the Zr-Ce split was obtained from the excess of the experimental points for the emission of 7 and 8 neutrons over the results of the fit shown in Fig. 8. The limiting ratio for the Ru-Xe split was estimated from the upper limits of the yields of the fragment pairs corresponding to emission of 8–10 neutrons.

D. Angular momenta of fission fragments

Average measured spins $\langle I_\gamma \rangle$ of the populated excited levels for ^{104}Mo and different Ba isotopes entering together into a succession of fragment pairs are given in Table VII. One can also see in this table average spins ($\langle I_\gamma \rangle$) of ^{144}Ba appearing in pairs together with the $^{106-104}$Mo partners. We believe that such a differentiation will be a good step in obtaining new results compared to those inferred from earlier experiments [53]. Having the results of the analysis presented in the previous section, one is able to know which primary fragments and in which proportion contributed to the formation of a detected fragment pair. From this we assigned to the fragments that appear in the first column of Table VII the mean numbers of neutrons ($\overline{\nu}$) evaporated from the primary fragments at their deexcitation (see last column of Table VII). Errors assigned to the values of $\overline{\nu}$ for the fragments of Mo and Ba appearing in the pairs of ^{104}Mo with ^{142}Ba, ^{140}Ba, and ^{138}Ba arise from the uncertainty related to the contributions of one of the three primary fragment pairs to the fission mode 2 (see the discussion above).

For the succession of three ^{144}Ba fragments, that come in pairs together with ^{106}Mo, ^{105}Mo, and ^{104}Mo, one observes a very low variation of $\langle I_\gamma \rangle$. Taking into account the growth of $\overline{\nu}$ along this chain of ^{144}Ba fragments and assuming that one evaporated neutron reduces the fragment angular momentum on average by one unit of $\hbar$, we find that a positive correlation shows up between the angular momentum of primary fragments and their excitation energy. This result is in agreement with what was inferred from models which rely upon the statistical equilibrium between collective degrees of freedom (see [52,53]). The picture appears to be more complicated in the case of the chain of ^{104}Mo fragments coming in pairs together with different Ba fragments. One observes a weak variation of $\langle I_\gamma \rangle$ for the ^{104}Mo fragments detected in the series of fragment pairs formed after evaporation from 1 to 6 neutrons (see Fig. 9). Again, after a correction for the effect of neutron evaporation, one will see for this sequence

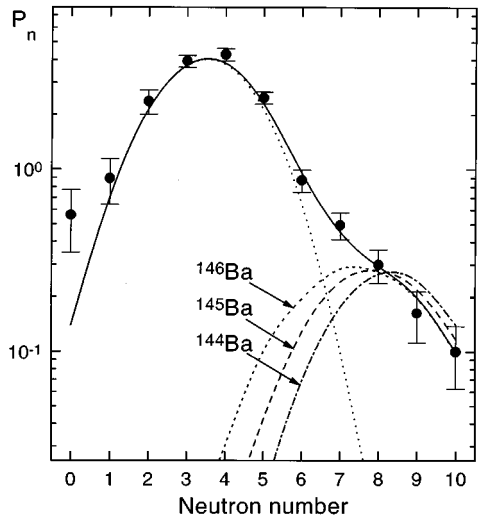

FIG. 7. Results of the unfolding procedures for our experimental total neutron multiplicity distribution of prompt fission neutrons (solid circles) for the Mo-Ba split (see also Fig. 3). The curves show the results of different unfolding procedures (see comments to curves in Fig. 6).

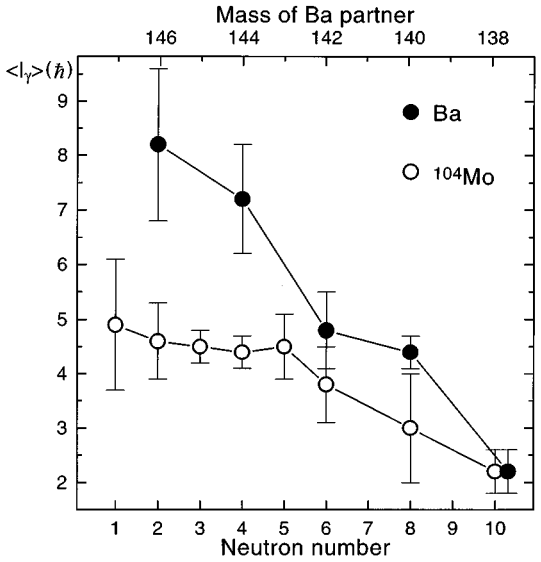

FIG. 9. Average angular momentum values $\langle I_\gamma \rangle$ are shown for levels populated in ^{104}Mo (open circles) and in complementary Ba fragments (closed circles) in function of the total number of prompt fission neutrons. These Mo and Ba isotopes are obtained in one succession of fragment pairs of ^{104}Mo-^{A}Ba formed as a result of emission of different numbers of prompt neutrons. The mass numbers of the secondary (obtained after neutron evaporation) Ba fragments are given in an upper scale.

a positive correlation between the angular momentum of primary fragments and excitation energy. However, two points in Fig. 9 associated with the pairs involving ^{140}Ba and ^{138}Ba, the 8 and 10 neutron evaporation partners of ^{104}Mo, completely drop out from this correlation. We consider this observation as an additional argument in support of the concept of two distinct fission modes discussed above. Indeed, in the framework of this concept, 100% of the yield of these two fragment pairs (see Table III) are from the second mode which contributes only 13% to the yield of the ^{104}Mo-^{142}Ba pair. Mode 2's contributions steeply decrease when one proceeds to other heavier Ba pairs of the sequence. Therefore one cannot exclude a supposition that the second fission mode results in lower angular moments of ^{104}Mo fragments. A reason for this might be a difference in the dynamic paths inherent to these two fission modes.

Angular momentum values of Ba fragments detected in pairs together with the ^{104}Mo partner are also shown in Fig. 9. For these Ba fragments the mean number of evaporated neutrons ($\overline{\nu}$) varies over a considerably wider range than in the case of the ^{104}Mo fragments shown in Fig. 9. This wider range appears mostly from ^{140}Ba and ^{138}Ba formed after neutron evaporation from highly excited primary Ba fragments which are related to mode 2. Adding the mean angular momentum values that these neutrons take from the nucleus, one comes to a rather high mean angular momentum of the primary Ba fragments ($\geqslant 10$). Perhaps, this does not look surprising because, according to the concept of a statistical equilibrium between the collective degrees of freedom at scission, the huge deformation of ^{146}Ba inferred for the second fission mode is connected with higher angular momentum of this fragment.

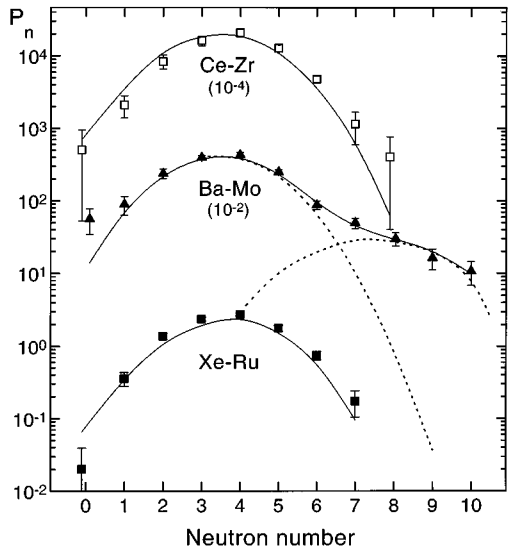

FIG. 8. Our experimental neutron multiplicity distributions for Ru-Xe, Mo-Ba, and Zr-Ce charge splits are shown along with the results of the unfolding procedures (dashed curve) described in the end of Sec. III C.

IV. CONCLUSIONS

A method based on measurements of intensities of γ transitions from correlated pairs of secondary fragments in a γ-γ-γ coincidence experiment was used for the first time to determine detailed characteristics of the spontaneous fission

of ^{252}Cf. By applying this method, we measured directly the yields of 139 particular pairs of fragments of five charge splits emerging in the spontaneous fission of ^{252}Cf. By summing up these yields, we obtained the mass, charge, and neutron multiplicity distributions of fission fragments, data that for a long time have been obtained only by using earlier integral methods to study low-energy fission. The agreement of our data with those which were known previously proves the validity of the approach made in this work. In some aspects (independent yields of fission fragments, mean neutron multiplicity obtained for different charge splits) our results complement considerably the previously known data. In addition, an approach used in this work allowed us to obtain yields and multiplicity distributions of prompt neutrons emitted at various charge splits, data unaccessible using previous methods. The attractive feature of these new distributions is that they were obtained, practically, as a result of direct measurements of the γ-γ coincidence peaks. This makes a strong difference between these distributions and those which are derived from the neutron detection experiments involving sophisticated unfolding procedures applied to the raw data. One particular important result of the approach is that it demonstrated that the high multiplicity neutron events known earlier for 7–9 neutron emission in the spontaneous fission of ^{252}Cf are to a large extent associated only with the Mo-Ba split.

Data on yields of fragment pairs provide the most direct information that allows one to investigate the excitation energy of primary fragments and derive their mass and charge distributions. That this really can be done is shown in this work for the cases of the Ru-Xe, Mo-Ba, and Zr-Ce charge splits of ^{252}Cf. We have established the observation of two distinct fission modes for the Mo-Ba charge split. A result is that mode 2 shows a very low value of $\langle$TKE$\rangle$ (very low Coulomb excitation) and a very narrow mass distribution around $A_L=106$, $A_H=146$ compared to the broad double bumped distribution of the normal fission of ^{252}Cf. It is possible that only one mass split, ^{106}Mo-^{146}Ba, ^{107}Mo-^{145}Ba, or ^{108}Mo-^{144}Ba is responsible for this mode, but some combination of these three fragments is also possible for mode 2 from the analysis of our data. The principal difference between mode 1 and mode 2 is that the mean excitation energy of the Ba fragments, ^{146}Ba, ^{145}Ba, and/or ^{144}Ba being ''normal'' in the case of the first mode, becomes enormously high when the second mode is realized. In mode 2 the barium nucleus is hyperdeformed with a long to short axis ratio of the order of 3:1 at scission. One encounters here a new situation earlier unknown in nuclear fission where one and the same fragment is formed in two fission modes that are unlike each other because of the very large scission point elongation of the heavy fragment in mode 2 as compared to its ''normal'' elongation in the case of mode 1.

The new generation of large multi Ge detector systems (Gammasphere, EUROGAM, GASP) provide better conditions for these kinds of experiments. With these detector systems, one can considerably increase the volume of data on the yields of fission fragment pairs. More complete data sets, similar to those given in Tables I–V but including more pairs and extended to more rare fragment pairs, will be realized. Then one will be able to draw more unambiguous conclusions about the primary fission fragments. The progress in the investigation of the levels scheme populated in fission will make possible the observation of similar results for the odd-odd charge splits. Already preliminary results from the early implementation of Gammasphere with only 36 Ge detectors have confirmed (Ref. [82]) the results reported here in Table III. More detailed studies are underway with data from the expanded Gammasphere (72 detectors).

A natural continuation of this study could be experiments involving the observation of γ-ray coincidences in combination with measurements of the fission fragment TKE and mass asymmetry. The measured TKE will be an important piece of information that will improve the conditions of the procedures intended to unfold the primary fragment excitation energy and mass distributions. This will considerably improve our ability to recognize the scission configurations and draw more precise conclusions about the final energy partition at fission. New possibilities will arise for learning the level population patterns of fission fragments and, therefore, new insights into the problem of the fragment angular moment origin will come.

ACKNOWLEDGMENTS

Two of the authors (G.M.T.-A. and A.V.D.) would like to express appreciation for the hospitality and financial support received during their stays at Vanderbilt University and Oak Ridge National Laboratory. This work was supported in part at Vanderbilt University and Idaho National Engineering Laboratory by the U.S. Department of Energy under Grant and contract Nos. DE-FG05-88ER40407 and DE-AC07-76ID01570, respectively; at the Joint Institute for Nuclear Research by Grant No. 94-02-05584-a of the Russian Federal Foundation of Basic Sciences; at the Institute of Physics of SASc by the Grant Agency of the SASc under Grant No. GA-SAV 517/1993. Oak Ridge National Laboratory is managed by Lockheed Martin Energy System, Inc., under Contract No. DE-AC05-84OR21400 for U.S. Department of Energy.

[1] G. M. Ter-Akopian, J. H. Hamilton, Yu. Ts. Oganessian, J. Kormicki, G. S. Popeko, A. V. Daniel, A. V. Ramayya, Q. Lu, K. Butler-Moore, W.-C. Ma, J. K. Deng, D. Shi, J. Kliman, V. Polhorsky, M. Morhač, W. Greiner, A. Sandulescu, J. D. Cole, R. Aryaeinejad, N. R. Johnson, I. Y. Lee, and F. K. McGowan, Phys. Rev. Lett. **73**, 1477 (1994).

[2] G. M. Ter-Akopian, J. H. Hamilton, Yu. Ts. Oganessian, A. V. Daniel, J. Kormicki, G. S. Popeko, A. V. Ramayya, Q.-H. Lu, K. Butler-Moore, W.-C. Ma, S. Ćwiok, W. Nazarewicz, J.-K. Deng, D. Shi, J. Kliman, M. Morhac, J. D. Cole, R. Aryaeinejad, N. R. Johmson, I. Y. Lee, F. K. McGowan, and J. X. Saladin, Phys. Rev. Lett. **77**, 32 (1996).

[3] R. Vandenbosch, in *Proceedings of the International Conference on Fifty Years Research in Nuclear Fission*, Berlin, Germany, 1989, edited by D. Hilsher, H. J. Krappe, and W. von Oertzen [Nucl. Phys. **A502**, 1 (1989)].
[4] J. J. Griffin, in *Proceedings of the Meeting 50 Years with Nuclear Fission*, Washington, D.C., Gaithersburg, Maryland, 1989, edited by J. W. Behrens and A. D. Carlson (American Nuclear Society, La Grange Park, Illinois, 1989), Vol. 1, p. 137.
[5] A. Mishaudon, in *Proceedings of the International Conference on the Fiftieth Anniversary of Nuclear Fission*, Leningrad, USSR, 1989, edited by L.V. Drapchinski (Khlopin Institute, St. Petersburg, 1992), Vol. 1, p. 167.
[6] F. Gönnenwein, in *The Nuclear Fission Process*, edited by C. Wagemans (CRC Press, Boca Raton, 1991), p. 287.
[7] H. Nifenecker, C. Signarbieux, R. Babinet, and J. Poitou, *Proceedings of the 3rd IAEA Symposium on the Physics and Chemistry of Fission*, Rochester, 1973 (IAEA, Vienna, 1976), Vol. 2, p. 117.
[8] A. C. Wahl, At. Data Nucl. Data Tables **39**, 1 (1988).
[9] S. G. Nilsson *et al.*, Nucl. Phys. **A131**, 1 (1969).
[10] V. V. Pashkevich, Nucl. Phys. **A161**, 275 (1971).
[11] H. C. Pauli, T. Lederberger, and M. Brack, Phys. Lett. **34B**, 264 (1971).
[12] M. Bolsterli, E. O. Fiset, J. R. Nix, and J. L. Norton, Phys. Rev. C **5**, 1050 (1972).
[13] M. G. Mustafa, U. Mosel, and H. W. Schmidt, Phys. Rev. C **7**, 1519 (1973).
[14] J. F. Berger, M. Girod, and D. Gogny, in *Proceedings of the International Conference on Theoretical Approaches Heavy Ion Reaction Mechanisms*, Paris, France, 1984, edited by M. Martinot, C. Ngô, and F. Lepage [Nucl. Phys. **A428**, 23c (1984)].
[15] M. G. Itkis, V. N. Okolovich, A. Ya. Rusanov, and G. N. Smirenkin, Z. Phys. A **320**, 433 (1985).
[16] M. G. Itkis, V. N. Okolovich, and G. N. Smirenkin, in [3] [Nucl. Phys. **A502**, 243c (1989)].
[17] E. K. Hulet, J. F. Wild, R. J. Dougan, R. W. Lougheed, J. H. Landrum, A. D. Dougan, M. Schädel, R. L. Hahn, P. A. Bisden, C. M. Henderson, R. J. Dupzyk, K. Sümmerer, and G. R. Bethune, Phys. Rev. Lett. **56**, 313 (1986).
[18] D. C. Hoffman, in [3] [Nucl. Phys. **A502**, 21c (1989)].
[19] E.K. Hulet, in [4], Vol. 2, p. 533.
[20] U. Brosa, S. Grossman, and A. Müller, Z. Naturforsch. Teil **A41**, 1341 (1986).
[21] V. V. Pashkevich, Nucl. Phys. **A477**, 1 (1988).
[22] S. Ćwiok, P. Rozmey, A. Sobiczewski, and Z. Patyk, Nucl. Phys. **A491**, 281 (1989).
[23] P. Möller, J. R. Nix, and W. J. Swiatecki, Nucl. Phys. **A492**, 349 (1989).
[24] U. Brosa, S. Grossman, and A. Müller, Phys. Rep. **197**, 167 (1990).
[25] C. Budtz-Jørgensen and H.-H. Knitter, Nucl. Phys. **A490**, 307 (1988).
[26] P. Siegler, F.-J. Hambsch, J. P. Teobald, and J. van Aarle, in *Proceedings of the 2nd International Conference on Dynamical Aspects of Nuclear Fission*, Smolenice, Slovakia, 1993, edited by J. Krištiak and B. I. Pustylnik (JINR Report No. JINR E7-94-19, 1994), p. 115.
[27] J. van Aarle, W. Westmeier, R. A. Estelund, and P. Petzelt, Nucl. Phys. **A578**, 77 (1994).
[28] C. Wagemans, P. Schillebeeckx, and A. Deruytter, in [3] [Nucl. Phys. **A502**, 287c (1989)].
[29] C. Wagemans, L. Dematte, P. D'Hondt, S. Pomme, P. Schillebeeckx, and A. Deruytter, in [26], p. 89.
[30] B. D. Wilkins, E. P. Steinberg, and R. R. Chasman, Phys. Rev. C **14**, 1832 (1976).
[31] H. Märten, in [26], p. 104.
[32] M. Berlanger, A. Gobbi, F. Hanappe, U. Lynen, C. Ngô, A. Olmi, H. Sann, H. Stelzer, H. Richel, and M. F. Rivet, Z. Phys. A **291**, 133 (1979).
[33] H. Nifenecker, J. Phys. (France) Lett. **41**, 47 (1980).
[34] H. Nifenecker, G. Mariolopoulos, J. P. Bocquet, R. Brissot, C. Hamelin, J. Crançon, and Ch. Ristori, Z. Phys. A **308**, 39 (1982).
[35] J. P. Bocquet and R. Brissot, in [3] [Nucl. Phys. **A502**, 213 (1989).
[36] F. Gönnenwein, in [5], p. 182.
[37] M. Asghar, N. Boucheneb, M. Djebara, and G. Medkour, in [26], p. 215.
[38] F. Gönnenwein, in [3] [Nucl. Phys. **A502**, 159c (1989)].
[39] J. Trochon, G. Simon, and C. Signarbieux, in [4], Vol. 2, p. 313.
[40] F. Gönnenwein and B. Börsig, Nucl. Phys. **A530**, 27 (1991).
[41] J. L. Sida, P. Armbruster, M. Bernas, J. P. Bocquet, R. Brissot, and H. R. Faust, in [3] [Nucl. Phys. **A502**, 233c (1989)].
[42] F. Gönnenwein, J. Kaufmann, W. Mollenkopf, P. Geltenbort, and A. Oed, in [26], p. 10.
[43] E. Cheifetz, J. B. Wilhelmy, R. C. Jared, and S. G. Thompson, Phys. Rev. C **4**, 1913 (1971).
[44] R. Aryaeinejad *et al.*, Phys. Rev. C **48**, 566 (1993).
[45] J. H. Hamilton, K. Butler-Moore, A. V. Ramayya, W.-C. Ma, X. Zhao, Q. Lu, J. Kormicki, D. Shi, J. K. Deng, S. Zhu, J. D. Cole, R. Aryaeinejad, R. C. Greenwood, S. S. Harrill, N. D. Lohstreter, G. M. Ter-Akopian, Yu. Ts. Oganessian, G. S. Popeko, A. V. Daniel, J. Kliman, V. Polhorsky, M. Morhač, I. Y. Lee, N. R. Johnson, and F. K. McGowan, in *International School-Seminar on Heavy Ion Physics*, Dubna, Russia, 1993, edited by Yu. Ts. Oganessian, Yu. E. Penionzhkevich, and R. Kalpakchieva (JINR, Dubna, 1993), Vol. 1, p. 276.
[46] S. Zhu, X. Zhao, J. H. Hamilton, A. V. Ramayya, Q. H. Lu, W.-C. Ma, L. K. Peker, J. Kormicki, H. Xie, W. B. Gao, J. P. Deng, I. Y. Lee, N. R. Johnson, F. K. McGowan, C. E. Bemis, J. D. Cole, G. M. Ter-Akopian, and Yu. Ts. Oganessian, in *XV Nuclear Physics Symposium*, edited by P. Hess [Rev. Mex. Fis. **38**, 53 (1992)].
[47] J. H. Hamilton, G. M. Ter-Akopian, Yu. Ts. Oganessian, A. V. Daniel, J. Kormicki, G. S. Popeko, A. V. Ramayya, Q.-H. Lu, K. Butler-Moore, W.-C. Ma, S. Ćwiok, W. Nazarewicz, W. Greiner, A. Sandulescu, J.-K. Deng, D. Shi, J. Kliman, M. Morhac, J. D. Cole, R. Aryaeinejad, S. J. Zhu, B. R. S. Babu, N. R. Johnson, I. Y. Lee, F. K. McGowan, and J. X. Saladin, *Low Energy Nuclear Dynamics – LEND'95* (World Scientific, Singapore, 1995), p. 187.
[48] J. H. Hamilton, A. V. Ramayya, S. J. Zhu, G. M. Ter-Akopian, Yu. Ts. Oganessian, J. D. Cole, J. O. Rasmussen, and M. A. Stoyer, Prog. Part. Nucl. Phys. **35**, 635 (1995).
[49] G. M. Ter-Akopian, J. H. Hamilton, Yu. Ts. Oganessian, A. V. Daniel, J. Kormicki, G. S. Popeko, A. V. Ramayya, Q.-H. Lu, K. Butler-Moore, W.-C. Ma, J.-K. Deng, D. Shi, J. Kliman, M. Morhać, J. D. Cole, R. Aryaeinejad, S. Zhu, B. R. S. Babu, N. R. Johnson, I. Y. Lee, and F. K. McGowan, in *International*

Conference on Exotic Nuclei and Atomic Masses, ENAM 95, edited by M. de Saint Simon and X. Sorlin (Editions Frontiers, Gif-sur-Yvette, 1995), p. 383.

[50] G. M. Ter-Akopian, J. H. Hamilton, Yu. Ts. Oganessian, A. V. Daniel, J. Kormicki, G. S. Popeko, A. V. Ramayya, Q.-H. Lu, K. Butler-Moore, W.-C. Ma, J.-K. Deng, D. Shi, J. Kliman, M. Morhać, J. D. Cole, R. Aryaeinejad, S. Zhu, B. R. S. Babu, N. R. Johnson, I. Y. Lee, and F. K. McGowan, *International Conference on Nuclear Spectroscopy and Structure of Atomic Nucleus* [Izv. Ross. Akad. Nauk, Ser. Fiz. **60**, 162 (1996)].

[51] J. R. Nix and W. Swiatecki, Nucl. Phys. **71**, 1 (1965).

[52] J. O. Rasmussen, W. Nörenberg, and H. J. Mang, Nucl. Phys. **A136**, 456 (1969).

[53] J. B. Wilhelmy, E. Cheifetz, R. C. Jared, S. G. Thompson, H. R. Bowman, and J. O. Rasmussen, Phys. Rev. C **5**, 2041 (1972).

[54] J. F. Berger, M. Girod, and D. Gogny, in [3] [Nucl. Phys. A **A502**, 85c (1989)].

[55] B. A. Emellanov, L. P. Kabina, I. A. Kondurov, Yu. E. Loginov, P. S. Sushkov, Nucl. Instrum. Methods **178**, 555 (1980).

[56] A. V. Daniel *et al.*, to be submitted to Nucl. Instrum. Methods Phys. Res.

[57] K. Butler-Moore, J. H. Hamilton, A. V. Ramayya, S. Zhu X. Zhao, W.-C. Ma, J. Kormicki, J. K. Deng, W. B. Gao, J. D. Cole, R. Aryaeinejad, I. Y. Lee, N. R. Johnson, F. K. McGowan, G. M. Ter-Akopian, and Yu. Ts. Oganessian, J. Phys. G **19**, L121 (1993).

[58] K. Butler-Moore, R. Aryaeinejad, J. D. Cole, Y. Dardenne, R. G. Greenwood, J. H. Hamilton, A. V. Ramayya, W.-C. Ma, B. R. S. Babu, J. O. Rasmussen, M. A. Stoyer, S. Y. Chu, K. E. Gregorich, M. Mohar, S. Asztalos, S. G. Prussin, K. J. Moody, R. W. Lougheed, and J. F. Wild, Phys. Rev. C **52**, 1339 (1995).

[59] Q. H. Lu, K. Butler-Moore, S. J. Zhu, J. H. Hamilton, A. V. Ramayya, V. E. Oberacker, W. C. Ma, B. R. S. Babu, J. K. Deng, J. Kormicki, J. D. Cole, R. Aryaeinejad, Y. X. Dardenne, M. Drigert, L. K. Peker, J. O. Rasmussen, M. A. Stoyer, S. Y. Chu, K. E. Gregorich, I. I. Lee, M. F. Mohar, J. M. Nitschke, N. R. Johnson, F. K. McGowan, G. M. Ter-Akopian, Yu. Ts. Oganessian, and J. B. Gupta, Phys. Rev. C **52**, 1348 (1995).

[60] S. J. Zhu, Q. H. Lu, J. H. Hamilton, A. V. Ramayya, L. K. Peker, M. G. Wang, W. C. Ma, B. R. S. Babu, T. N. Ginter, J. Kormicki, D. Shi, J. K. Deng, W. Nazarevicz, J. O. Rasmussen, M. A. Stoyer, S. Y. Chu, K. E. Gregorich, M. F. Mohar, S. Asztalos, S. G. Prussin, J. D. Cole, R. Aryaeinejad, Y. K. Dardenne, M. Drigert, K. J. Moody, R. W. Loughheed, J. F. Wild, N. R. Johnson, I. Y. Lee, F. K. McGowan, G. M. Ter-Akopian, and Yu. Ts. Oganessian, Phys. Lett. B **357**, 273 (1995).

[61] W. R. Phillips *et al.*, Phys. Rev. Lett. **57**, 3257 (1986).

[62] M. A. C. Hotchkis *et al.*, Phys. Rev. Lett. **64**, 2123 (1990).

[63] W. R. Phillips *et al.*, Phys. Lett. B **212**, 412 (1988).

[64] A. S. Mawbray *et al.*, Phys. Rev. C **42**, 1126 (1990).

[65] M. A. C. Hotchkis *et al.*, Nucl. Phys. **A530**, 111 (1991).

[66] J. K. Tuli, Nucl. Data Sheets **69**, 69 (1993).

[67] T. Datta, S. P. Dange, S. K. Das, Satya Prakash, and M. V. Ramaniah, Z. Phys. A **324**, 81 (1986).

[68] J. F. Wild *et al.*, Phys. Rev. C **41**, 640 (1990).

[69] Yu. A.Lazarev *et al.*, Phys. Lett. **52B**, 321 (1974).

[70] D. C. Hoffman *et al.*, Phys. Rev. C **21**, 637 (1980).

[71] F.-J. Hambsch, H. -H. Knitter, and C. Budtz-Jøgensen, Nucl. Phys. **A554**, 209 (1993).

[72] I. D. Alkhazov *et al.*, in *International Conference on the Fifteenth Anniversary of Nuclear Fission*, Leningrad, USSR, 1989, edited by L. V. Drapchinski (Khlopin Institute, St. Petersburg, 1992), Vol. 2, p. 300.

[73] P. Lancaster and K. Salkauskas, *Curve and Surface Fitting—An Introduction* (Academic, New York, 1986).

[74] J. W. Schmidt and H. Späth, *Spline in Numerical Analysis* (Akademie-Verlag, Berlin, 1989).

[75] J. H. Hamilton, A. V. Ramayya, J. Kormicki, W. -C. Ma, Q. H. Lu, D. Shi, J. K. Deng, S. J. Zhu, A. Sandulescu, W. Greiner, G. M. Ter-Akopian, Yu. Ts. Oganessian, G. S. Popeko, A. V. Daniel, J. Kliman, V. Polhorski, M. Morhavˇ, J. D. Cole, R. Aryaeinejad, I. Y. Lee, N. R. Johnson, and F. K. McGowan, J. Phys. G **20**, L85 (1994).

[76] A. Sandulescu, A. Florescu, F. Carstoiu, W. Greiner, J. H. Hamilton, A. V. Ramayya, and B. R. S. Babu, Phys. Rev. C **54**, 248 (1996).

[77] P. G. Young, E. D. Arthur, and M. B. Chadwick (unpublished).

[78] R. Guin, S. K. Saha, and M. Uhl, Phys. Rev. C **46**, 250 (1992).

[79] F. M. Lanzafame and M. Blann, Nucl. Phys. **A142**, 545 (1970).

[80] D. Vinciguurra, K. Kotajima and R. E. Van de Vijver, Nucl. Phys. **77**, 337 (1965).

[81] W. Neumann, W. Woelfi, P. Heimgartner and R. M. Streicher, Nucl. Instrum. Methods Phys. Res. B **50**, 57 (1990).

[82] J. H. Hamilton, G. M. Ter-Akopian, A. V. Ramayya, J. Kormicki, B. R. S. Babu, Yu. Ts. Oganessian, A. V. Daniel, S. J. Zhu, M. G. Wang, J. K. Deng, W. C. Ma, T. N. Ginter, G. S. Popeko, Q. H. Lu, J. O. Rasmussen, S. Asztalos, I. Y. Lee, S. Y. Chu, K. E. Gregorich, A. O. Macchiaveli, M. F. Mohar, S. Prussin, M. A. Stoyer, R. W. Lougheed, K. J. Moody, J. F. Wild, J. D. Cole, R. Aryaeinejed, Y. K. Dardenne, and M. Drigert, in *Proceedings of the Workshop on Gammasphere Physics*, Berkeley, 1995, edited by M. Delaplanque-Stevens (World Scientific, Singapore, in press).